Time-resolved spectral and spatial description of laser-induced breakdown in air as a pulsed, bright, and broadband ultraviolet–visible light source

Antonio Borghese and Simona S. Merola

The optical breakdown induced in air at atmospheric pressure by Nd:YAG *Q*-switched laser pulses is studied in terms of the spectral features of the emitted radiation in the wavelength range 180–850 nm during the first 200 ns after the laser pulse onset. During the plasma build up, radiation emission features intense, broadband, and structureless ultraviolet–visible spectra before the appearence of atomic lines on the microsecond scale. Also, the emitting plasma kernel, imaged during the buildup and decay stages in the early tens of nanoseconds, turns out to have a size of ~0.3 mm and a volume of ~0.02 mm^3. The coupling of direct emission data and broadband absorption measurements allowed us to retrieve peak values of electron temperature above 100,000 K and of an optical depth of the order of unity, under the assumptions of local thermodynamic equilibrium and a homogeneous kernel. The simultaneous occurrence of such temporal, spatial, and spectral features of the plasma kernel suggests its exploitation as a pulsed, bright, and broadband ultraviolet–visible light source.

OCIS codes: 140.0140, 140.3460, 300.6540, 350.5400.

1. Introduction

In optical investigations of the chemical and physical properties of matter, lasers play a dominant role as light sources because of their well-known and peculiar temporal, spatial, and spectral features. Based on such characteristics, powerful optical techniques have been developed and applied in a wide variety of both fundamental and practical contexts.

As it happens, however, in some cases coherence of the electromagnetic radiating field is not strictly required, as in optical diagnostic techniques based on linear light–matter interactions, e.g., one-photon absorption and incoherent light scattering. In addition, lasers operate at just one or, at most, a few discrete wavelengths, either fixed or tunable. This quite obvious and intrinsic feature is a limiting factor in those cases for which light–matter interactions over a broadband spectral range would yield much more information than would monochromatic counterparts.

On the other hand, broadband light sources, such as deuterium or high-pressure xenon lamps driven by electrical discharges, best fulfill the requirements of broadband spectral emission, but their brilliance turns out to be far lower than required by *in situ* or remote-sensing applications. In this respect an ideal light source should simultaneously have the temporal and spatial features of lasers and the broadband emission of arc-based lamps; in short, it would be a white laser.

A practical and affordable solution would be an obviously incoherent light source that features substantial improvements over the most widely used high-pressure, pulsed xenon lamps in terms of its spectral, spatial, and temporal properties. Fast light emission would be achieved by means of transient plasmas, excited by suitable electrical circuitry.[1] In addition, instrument-oriented light sources should fulfill the requirements of cost effectiveness, reliability, and ease of handling. Such constraints prevent interesting and powerful solutions, such as z-pinches, sliding-spark discharges, and picosecond-pulse sources, from being considered, for either technical or practical reasons. Recently, substantial enhancements of temporal and spectral properties were achieved by fast pulsing of commercial xenon lamps.[2]

In this paper we propose that a light source approaching these ideal features is the emitting plasma kernel that results from the optical breakdown in a

The authors are with the Istituto Motori, Consiglio Nazionale delle Ricerche, Via Marconi 8, I-80125 Napoli, Italy.

Received 6 October 1997; revised manuscript received 4 March 1998.

0003-6935/98/183977-07$15.00/0

gaseous medium induced by a Q-switched laser pulse. The phenomenon of optical breakdown initiated and sustained by pulsed laser radiation has been known since the advent of the first pulsed laser sources in the early 1960's.[3] In more recent years an extensive literature has addressed a variety of properties and applications of such physical effects induced on solid targets,[4–6] research driven by studies on controlled nuclear fusion by means of inertial confinement.

The present study is purposely restricted to considering the optical breakdown as a light source in itself, featuring temporal, spatial, and spectral properties that are relevant in the field of optical diagnostics, applied primarily but not exclusively to investigate combustion processes, to detect combustion by-products, and ultimately to monitor environmental pollution.

In what follows, we describe this light source in terms of its spectral, temporal, and spatial behavior. A first-order analysis of the plasma, assumed to be in local thermodynamic equilibrium (LTE), is also provided, resulting in the estimate of the electron temperature as function of time within the first 100 ns after laser onset.

2. Experimental Setup

Optical breakdown in air has been obtained with a Q-switched Nd:YAG laser source operated at $\lambda = 1.06$ μm, with 200 mJ of energy/pulse, a 7-ns pulse duration, and an 8-mm beam diameter; the laser pulse is focused by a 20-mm focal-length high-power lens in air at STP conditions. The light emitted by the resulting plasma is brought to the 50-μm input slit of a flat-field spectrometer, equipped with either a 200 grooves/mm holographic grating for spectral analysis in the ultraviolet–visible 250–850 nm wavelength range or a 360 grooves/mm grating for higher spectral resolution in the 180–400 nm ultraviolet band.

Detection and acquisition of spectra are carried out by means of a multichannel intensified and gateable 1024-photodiode array (PDA) detector. Time-resolved measurements are made by means of a delay generator, providing the desired time delays from the laser pulse onset to a pulse generator, which drives the microchannel-plate intensifier of the PDA detector. The overall time resolution of the acquired signals is determined by the 5-ns gating pulses of the microchannel plate. Wavelength calibration of the spectrometer–detector assembly are carried out by means of a mercury spectral lamp, whereas the overall spectral response in the range 180–450 nm is obtained by means of a D_2 lamp and related ordinary procedures.

Acquisition proceeds either on a single-shot basis or by averaging over many shots to reduce the signal noise. The shot-by-shot fluctuation of the light emitted by the plasma turns out to be smaller than that of the laser pulse, which is ~3%. Experimental data reported here all refer to averages (summations) of 20 shots; averaging reduces the shot noise to below 1%.

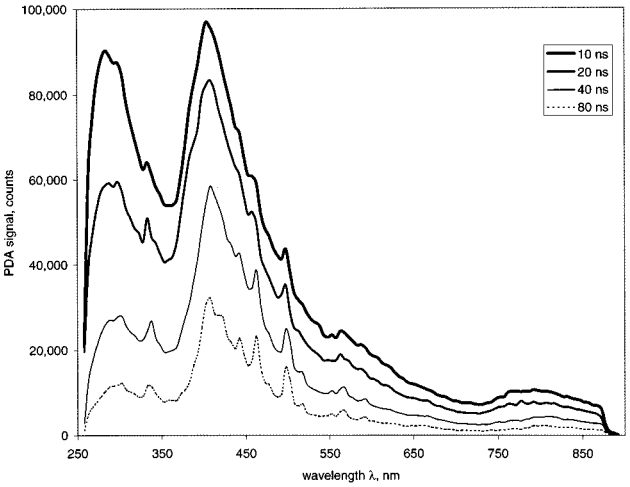

Fig. 1. PDA signal spectra of the light emitted by laser-induced breakdown dispersed by a 200 groove/mm grating at 10, 20, 40, and 80 ns after laser onset.

3. Results

The characterization of the plasma arising from the laser-induced optical breakdown of air has been carried out in terms of (a) spectral dispersion of the ultraviolet–visible light emission and of (b) spatial imaging of the plasma, both as functions of time during the first 100 ns from the laser pulse onset, with a time increment of $\Delta t = 2$ ns and with an overall time resolution of 5 ns, as determined by the gate of the microchannel-plate intensifier.

Spectral analysis. Figure 1 shows four PDA signal spectra, reported in arbitrary units (counts), of the light emitted by laser-induced breakdown in laboratory air in the spectral range 250–850 nm and acquired at 10-, 20-, 40-, and 80-ns time delays after the laser pulse onset. The spectral shapes in Fig. 1 are strongly affected by instrumental response, mainly by the dispersing grating and the intensifier photocathode, which determines the strong signal levels of the broad band around 400 nm. The highest signal levels are achieved in the first nanoseconds, when the spectrum extends over the full ultraviolet–visible spectral window and shows a nearly structureless shape, with two broad maxima at ~270 and 400 nm. At later times, the signal intensities in the ultraviolet range decrease faster than in the visible band, where instead isolated lines and structured bands appear as a result of the relaxation of plasma toward lower electron temperatures and densities. In Fig. 1 signals in the wavelength range 250–500 nm are derived exclusively from the first order of the dispersing grating; above this range they are affected additively by the second order, which contributes at wavelengths larger than 2×250 nm = 500 nm, and by the third order above 3×250 nm = 750 nm.

Further investigations have been restricted to the spectral range 180–400 nm, where the plasma emits most of the radiation energy detectable in our experiments. In this case a 360 groove/mm grating was

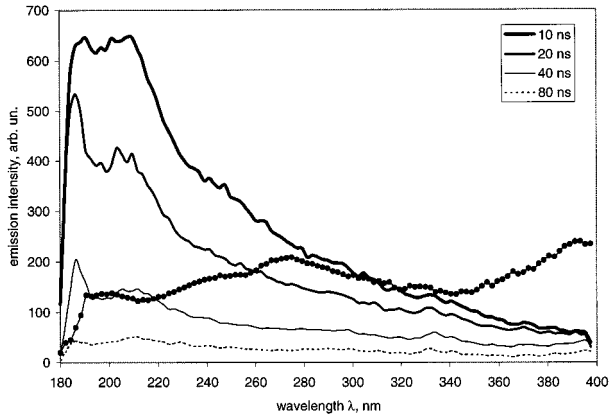

Fig. 2. Emission spectra dispersed by a 360 groove/mm grating at 10, 20, 40, and 80 ns after laser onset and corrected by instrumental response (filled circles).

used, which nearly doubles the spectral resolution. Also, the resulting spectra have been corrected for instrumental response, which is given by the ratio of the spectrum acquired from the D_2 lamp and its calibrated spectral emission and is shown as the curve with filled circles in Fig. 2.

Figure 2 also shows emission spectra, corrected for the instrumental response, in the wavelength range 180–400 nm, at increasing time delays from the laser pulse onset; heavier curves correspond to shorter delays as indicated. The resulting spectral shapes are smooth, peak near $\lambda = 200$ nm, and show noticeably strong signals down to the far-ultraviolet region. The sharp decrease below 200 nm is due to a drop in the overall detector response. Neither emission lines nor structured bands are observed in this spectral range.

Figure 3 shows the normalized signal intensities at the indicated wavelengths as functions of time within the first 200 ns. Each curve in Fig. 3 has been obtained from spectra, like those shown in Fig. 2, acquired at increasing delay times ($\Delta t = 2$ ns) from the laser pulse onset and then reported as a function of time, with the chosen wavelength held constant. At $\lambda = 200$ nm, the apparent rise and fall times of the signals are of the order of 10 ns, whereas the fall time is longer for longer wavelengths. Since the time resolution of the acquired signals is determined by the finite gate pulse duration (5 ns), the real rise and fall times turn out to be shorter than those observed, approaching the corresponding times of the laser pulse; as a result, the duration (FWHM) of the light emission can be estimated to be less than 20 ns.

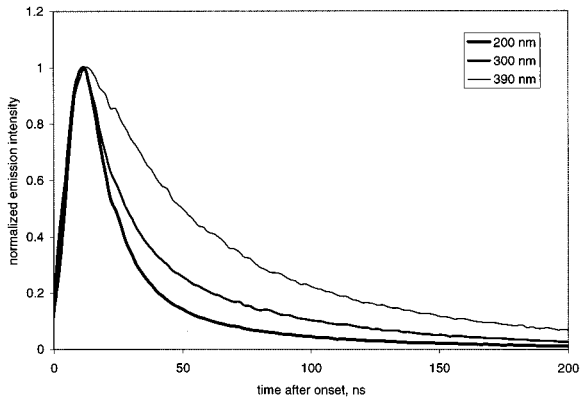

Fig. 3. Normalized signal intensities as functions of time, emitted at wavelengths $\lambda = 200$, 300, 390 nm.

Spatial analysis. The data of Figs. 1, 2, and 3 represent spectrally resolved emission intensity measurements, which turn out to be integrated over the whole spatial extent of the plasma kernel, however. To provide a spatially resolved description of the emitting volume, a set of measurements was carried out with the spectrometer removed, so that the PDA was used as a one-dimensional imaging camera, with the resulting light intensities being spectrally integrated. The plasma kernel was then imaged onto the PDA plane by a quarz lens mounted to give a 20× magnification; the PDA was masked by a horizontal 100-μm slit. As a result, for each vertical position of the lens, linear image elements (horizontal strips) were acquired at increasing delay times. The acquisition was repeated at increasing vertical y positions of the lens, so that a three-dimensional array $I(x, t, y)$ was built and stored. Data were then plotted in the form of two-dimensional arrays $I_t(x, y)$ for chosen delay times t from the laser pulse onset. Figure 4 shows a selection of eight images of the plasma kernel, with the intensity z scale traced by gray levels; the images correspond to the indicated time delays. In Fig. 4 the laser beam enters from the right-hand side and is brought by the high-power lens into the nominal focus at $x = 0$, $y = 0$. It appears from Fig. 4(a) that the plasma is initiated in a region close to but clearly upstream the nominal focus, where the conditions of optical breakdown occur first. Soon after [see Figs. 4(b)–4(d)] an apparent right shift of the plasma emission occurs with an extremely high instantaneous speed, of the order of 10^4 m/s. This upstream shift results from the buildup of a laser-driven plasma combustion wave that travels against the incoming laser beam, whereas the opposite side, obscured by the absorbing plasma, is no longer fed by the laser energy and relaxes through deexcitation of the ionized species. The observed shift ceases ~10 ns from the onset of the phenomenon, which corresponds to the end of the laser pulse; at this stage the emission intensity reaches its maximum value, from which it decays in times as short as a few tens of nanoseconds. During the stage of maximum emission the shape of the plasma kernel, although irregular, can be considered to be elliptical, with a minor (vertical) axis $a_y \sim 0.3$ mm and a major (horizontal) axis $a_x \sim 0.4$ mm, evaluated at 50% of the peak emission intensity; this results in a plasma volume $v_p = (\pi/6 \times a_y^2 \times a_x)$ of ~0.02 mm^3.

4. Discussion

The volume of the plasma kernel in our experiments was measured to be of the order of 0.02 mm^3. Assuming, as a rule of thumb, nearly full absorption (i.e.

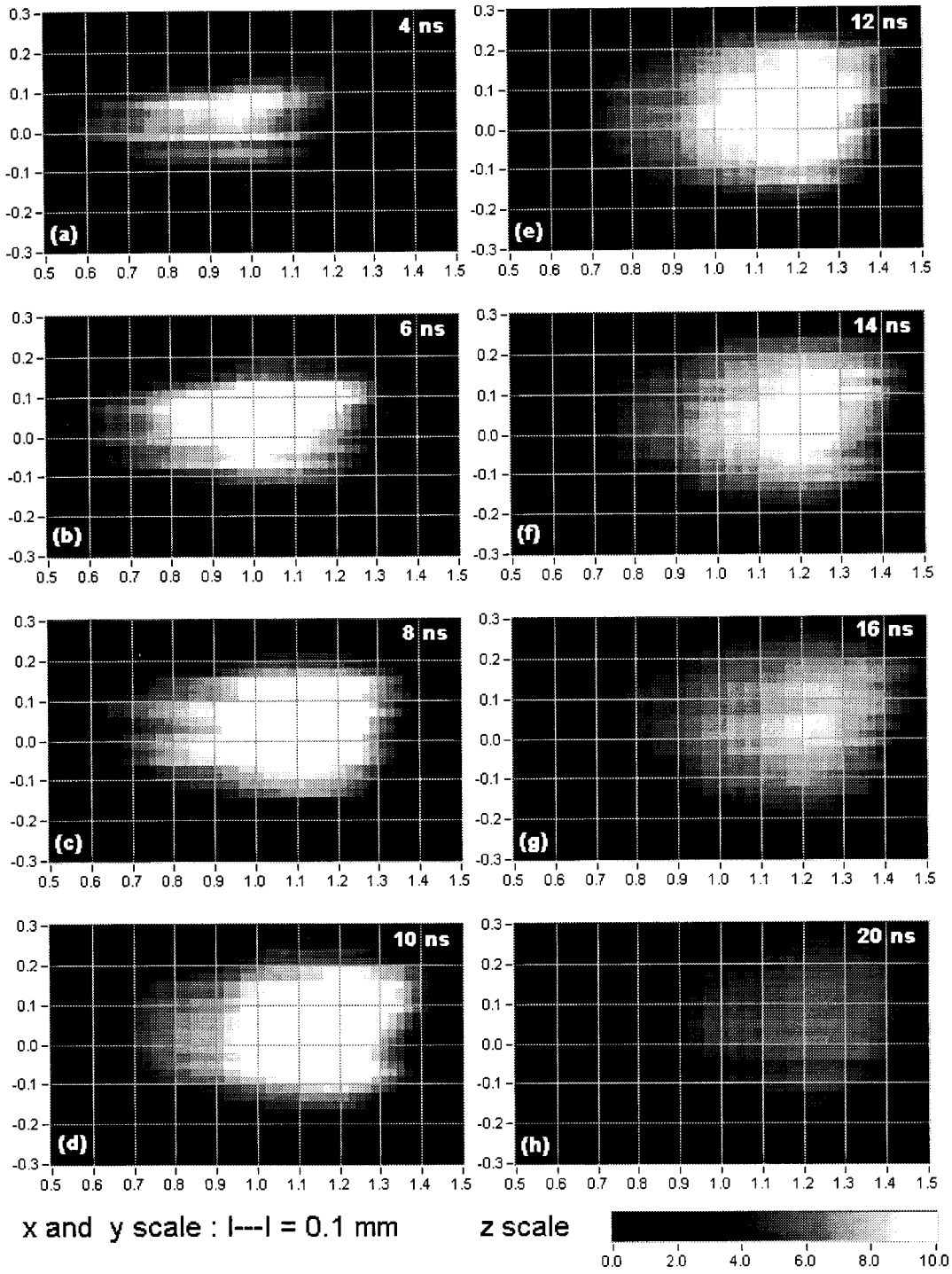

Fig. 4. Selection of eight images of the plasma kernel recorded at time delays of (a) 4, (b) 6, (c) 8, (d) 10, (e) 12, (f) 14, (g) 16, and (h) 20 ns after laser onset. The laser beam travels from right to left (nominal focus at $x = 0$, $y = 0$).

neglecting reflections, if any) of the 200-mJ incident laser energy, delivered in 10 ns, the resulting average energy density per unit volume is 10^4 J/cm^3, and the corresponding power density is of the order of 10^{12} W/cm^3. Such an extremely high level of internal energy pushes the gaseous medium into ionized conditions that are by far more intense than those in what are ordinarily referred to as laboratory plasmas.[1,3,7] Indeed, the first observations of the phenomenon at still higher laser energy and power levels revealed production of x rays and electron temperatures in excess of $\sim 10^6$ K.

From the point of view in this work, the laser-fired plasma kernel can be considered to have three important physical properties simultaneously: (a) a broadband emission continuum, spreading over the ultraviolet–visible electromagnetic spectrum and which is particularly intense in the far-ultraviolet

region; (b) a very small size, of the order of few hundreds of micrometers, determined by the focused laser beam; the smallness implies a high brilliance (power or energy per unit area of the emitting surface) and a rather low divergence angle when the beam is collimated; (c) a very short duration, of the order of few tens of nanoseconds, which approaches that of typical Q-switched laser sources.

Emission spectra recorded within the first tens of nanoseconds show neither isolated lines nor structured bands emerging from the strong broadband continuum. This situation is distinctive of optically thick plasmas and, in terms of plasma parameters, implies unusually high values of the electron density and, if LTE can be assumed, of the electron temperature.[8,9] The existence of LTE would allow an easier and more detailed analysis of the plasma to be performed.

On the one hand, the observed plasma kernel features very strong spatial gradients and extremely fast transients, conditions that even separately tend to imply departure from LTE conditions, at least within the early stages of the plasma lifetime. On the other hand, there are reasons that LTE is likely to occur. First, the optical thickness of the plasma implies a partial reabsorption of emitted energy, thus reducing the effective weight of the radiative decay compared with that for collisional transitions; such a situation relaxes the conditions for the establishment of a Maxwell's distribution of electrons velocities. Also, the extremely high internal energy density of the plasma kernel involves correspondingly large values of the local pressure, which again helps LTE to be established very quickly. In what follows, as a first-order attempt to describe the plasma, the LTE hypothesis, although questionable, will be assumed.

Following Griem,[8] in a collision-dominated, optically thick, LTE plasma the effective absorption coefficient $k'(\lambda, x)$, given by the difference between true absorption and induced emission, and the emission coefficient $\varepsilon(\lambda, x)$, which accounts for spontaneous transitions, at the wavelength λ and at the spatial position x within the plasma, are related by Kirchhoff's law:

$$\varepsilon(\lambda, x) = k'(\lambda, x) I_T(\lambda, x). \tag{1}$$

$I_T(\lambda, x)$ is the emission intensity of a blackbody at the electron temperature T, given by the Kirchhoff–Planck function

$$I_T(\lambda) = (2hc^2/\lambda^5)[\exp(hc/\lambda kT) - 1]^{-1}, \tag{2}$$

where λ, c, h, and k are the radiation wavelength, the speed of light, and Planck's and Boltzmann's constants, respectively.

Now the emitted radiation can be derived by our considering the spatial gradient of the intensity along the line of sight, which is determined by the difference between emission and absorption, namely,

$$\mathrm{d}I(\lambda, x)/\mathrm{d}x = \varepsilon(\lambda, x) - k'(\lambda, x) I(\lambda, x). \tag{3}$$

Integration of the equation of radiative transfer (3), taking into account relationships (1) and (2), can be accomplished only in special cases, depending on the optical thickness of the plasma.

In optically thin plasmas, that is, when $\varepsilon(\lambda, x) \gg k'(\lambda, x) I(\lambda, x)$, the solution is straightforward, and for axially symmetric kernels Abel's integral inversion can be applied to retrieve the corresponding $I(\lambda, r)$ quite easily. The procedures for optically thick plasma are less manageable, since, in addition to the existence of large spatial gradients and fast transients, redistribution of radiant energy emitted from given points and reabsorbed in adjacent layers leads to nonlinear integrodifferential equations and, in any case, to uncontrolled uncertainties. Thus, within the limits of the present simplified treatment, we invoke the further assumption of a spatially uniform plasma, which means that ε, k' and I_T do not depend on x, so that the plasma is treated as a homogeneous kernel of characteristic size d. Equation (3) can be then integrated to give

$$I(\lambda) = I_T(\lambda)[1 - \exp(-k'd)]^{-1}, \tag{4a}$$

where $k'd$ is the optical depth of the plasma and $I(\lambda)$ is the experimentally observed spectral intensity emitted by the plasma.

For $I_T(\lambda)$ and hence T to be evaluated from Eq. (4a), the optical depth $k'd$ as a function of wavelength must be determined. To this end an absorption measurement is needed, which involves the use of a comparison light source, of known emission intensity $I_c(\lambda)$, placed behind the observed plasma. In this case the total intensity $I'(\lambda)$ is given by

$$I'(\lambda) = I(\lambda) + I_c(\lambda)\exp(-k'd). \tag{4b}$$

After simple manipulation, the system of Eqs. (4a) and (4b) yields

$$k'd = \log\{I_c(\lambda)/I'(\lambda) - I(\lambda)]\}, \tag{5a}$$

$$I_T^{\exp}(\lambda) = I(\lambda) \times I_c(\lambda)/[I(\lambda) + I_c(\lambda) - I'(\lambda)]. \tag{5b}$$

In our experiments the plasma itself has been used as a comparison light source, with a flat metal mirror placed behind the plasma kernel. Actually, the spectra $I'(\lambda)$ and $I(\lambda) + I_c(\lambda)$ in Eqs. (5a) and (5b), are obtained by our aligning the mirror so that the reflected image lies on or off, respectively, the line of sight determined by the plasma kernel and the spectrometer input slit. According to Eq. (4b), the intensity $I'(\lambda)$ is given by the sum of the direct plasma emission $I(\lambda)$ and the reflected (and attenuated by the plasma) term $I_c(\lambda)\exp(-k'd)$. The plasma is used to probe itself.

Under the assumed hypotheses of LTE and a homogeneous kernel, $I_T^{\exp}(\lambda)$ in Eq. (5b) represents the experimentally derived Planck function, which is to be compared and fitted with its theoretical expression (2), to derive the best value of the parameter T. The intermediate results of such procedure are given in Fig. 5, which, for reference and in arbitrary units, shows an acquired spectrum $I(\lambda)$ (thin solid curve)

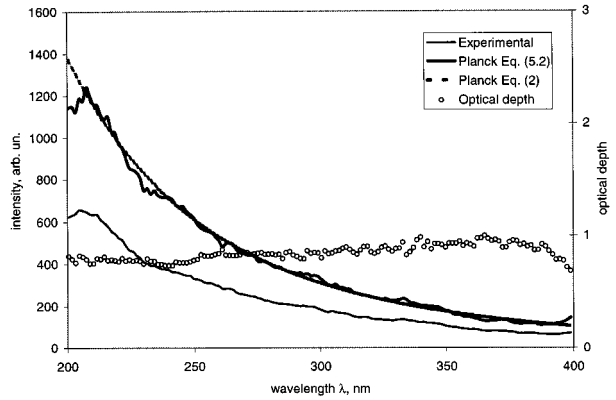

Fig. 5. Thin solid curve, emission intensity spectrum acquired at $t = 10$ ns; thick solid curve, intensity spectrum as evaluated from Eq. (5b); open circles, optical depth of plasma as evaluated from Eq. (5b); dashed curve, Planck function in Eq. (2) evaluated for $T = 103{,}000$ K.

corrected for the instrumental response and emitted 10 ns after the laser pulse onset. The corresponding optical depth $k'd$, evaluated from Eq. (5a), is shown in Fig. 5 (open circles) as function of the wavelength. Figure 5 also shows the associated blackbody intensity $I_T^{\exp}(\lambda)$ as evaluated from Eq. (5b) (thick solid curve) as function of the wavelength.

An error analysis of processed data shows that the values of the optical depth derived from Eq. (5a) and the values of the experimentally determined Planck function in Eq. (5b) are at most 15% and 7%, respectively. Finally, the best fit to this spectrum of the analytical Planck function [Eq. (2)], determined with an accuracy of $\pm 6\%$, is shown by a dashed line and corresponds to a value of temperature $T = 103{,}000$ K. Also, the plasma turns out to have a moderate optical depth ($k'd$ in the range 0.8–1.0) and to radiate essentially as a gray body in the spectral range considered.

Similar numerical processing of the experimental data has been carried out at different delays from the laser pulse onset. The results are reported in Fig. 6,

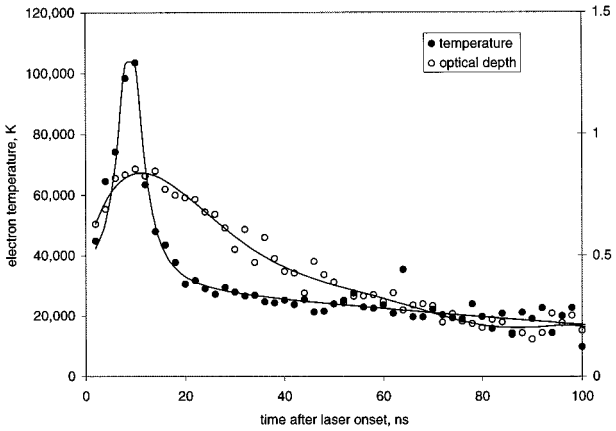

Fig. 6. Time behavior of plasma electron temperature (filled circles) and spectrally averaged optical depth (open circles) evaluated as in Fig. 5 (see text).

which shows the electron temperature (filled circles), evaluated as described above, as a function of time. The electron temperature T builds up with a very short rise time, corresponding to laser pumping action, and reaching values above 100,000 K. Soon after, the plasma cools through two distinct stages, the first with a time constant of a few nanoseconds, corresponding to free–free and free–bound transitions, and the second with a much longer fall time, of the order of hundreds of nanoseconds and related to species recombination (free–bound and bound–bound transitions). Figure 6 also shows the time behavior of the spectrally averaged optical depth, which ranges from nearly unity at early stages down to ~ 0.2 at 100 ns.

In summary, the reported temporal, spectral, and spatial features of light sources, based on laser-induced air breakdown, compare favorably with the corresponding properties of those driven by electrical gas discharges (see, e.g., Refs. 1, 2, and 7). First, the emission spectrum is by far more pronounced in the ultraviolet region, owing to the much higher electron density and temperature achieved. Also, the laser-induced breakdown allows one to deliver to the gaseous medium amounts of excitation energy of the order of joules within few nanoseconds; this is to be compared with only a few millijoules delivered on the same time scales by electrical discharges, for which intrinsic stray inductance limits the energy transfer from the circuit to the gas. In addition, the shape of the laser-excited plasma is nearly spherical, with emitting volumes of $\sim 10^{-2}$ mm^3, whereas electrical discharges occur with mostly cylindrical shapes and corresponding volumes of the order of 1 mm^3. This implies a much higher focusability of the plasma's emitted light or more confined propagation over large distances, as appropriate.

Finally, we note that further improvements of the reported features might be achieved by optimizing the light source operating conditions, e.g., gas composition and pressure, laser pulse duration, and focusing optics.

5. Applications

As of this writing, the laser plasma described in this paper has been used as the light source in three different experiments, briefly reported below, each providing deeper insights into the field involved.

In the first experiment, ultraviolet–visible spectrophotometry carried out in the 190–500-nm wavelength band over a 100-m-long optical path allowed us to identify and measure selectively and simultaneously the volume concentrations of the major gaseous and particulate pollutants (NO, NO_2, one-, two-, and three-ring aromatic hydrocarbons, and soot) in the air-diluted exhaust emitted from internal-combustion engines, with ten parts per billion (parts in 10^9) sensitivity for single-shot operation.[10] Analougous measurements carried out with a commercial pulsed high-pressure xenon lamp showed much lower sensitivity because of its vanishing light emission below 250 nm.

Second, ultraviolet scattering–extinction spectroscopy experiments carried out on water-trapped combustion by-products allowed us to detect carbonaceous nanoparticles with retrieved sizes in the range 2–4 nm; particles were found at comparable concentrations in both spark-ignited and compression-ignited engines exhausts.[11]

In a third experiment, dealing with spray drying processes of 100-μm-sized droplets of metal-nitrate aqueous solutions, the thermal history and the physicochemical transformations of single droplets were reconstructed from spectrally resolved analysis of the ultraviolet light scattered by single droplets on a single-shot basis.[12]

In all the cases cited above, the features of the light source either allowed us to develop new experimental techniques or enhanced the sensitivity of the experiments, relative to conventional light sources.

6. Conclusions

We have reported the time-resolved (early 200 ns) spectral and spatial features of the ultraviolet–visible radiation of the plasma kernel generated by laser-induced optical breakdown in air at ambient temperature and pressure conditions. The plasma spectral behavior has been described at two different spectral dispersions, showing that the emission spectrum is wide, structureless, and particularly intense in the far ultraviolet region, resulting in substantial improvement over existing light sources.

The shape of the plasma turned out to be irregular during the formation stage and nearly elliptical at later times, with a spatial extent of 0.3–0.4 mm, involving a volume of the order of 0.02 mm^3. A plasma combustion wave, traveling toward the incoming laser beam, is evident within the first nanoseconds, driven by the pumping laser radiation. The temporal evolution of the plasma emission shows a very fast and intense emission pulse, lasting $\sim$10 ns, followed by a relatively long tail, with a characteristic decay time of hundreds of nanoseconds.

Under the assumptions of (a) LTE and (b) a homogeneous kernel, a simplified plasma model has been described on the basis of experimental data. The model allowed us to evaluate the optical depth and the electron temperature of the plasma as functions of wavelength within the first 100 ns following the pumping laser pulse. Optical depth valued in the range 0.2–1.0 and nearly gray-body behavior have been inferred. Also, the electron temperature as a function of time has been derived, reaching values as high as 100,000 K after $\sim$10 ns after plasma onset.

The features reported above are relevant for applications, since they demonstrate that the plasma kernel produced by laser optical breakdown can be considered a particular pulsed, bright, and broadband ultraviolet–visible light source. As such, it can be used advantageously in applications for which ordinary arc-based lamps are not suitable enough because of their duration, spectral emission, or their lack of brightness, as well as in some optical diagnostic configurations for which the need of a broadband operation prevent lasers from being usefully exploited.

The authors acknowledge the stimulating discussions and encouragement of A. D'Alessio and M. Diana and the helpful assistance in the experiments of G. Cantilena.

References

1. F. B. A. Früngel, *High-Speed Pulse Technology* (Academic, New York, 1965).
2. S. Itami and T. Araki, "An intense, broadband emission spectrum, thyratron-gated nanosecond light source using a commercially available Xe short-arc lamp," Rev. Sci. Instrum. **67,** 3035–3038 (1996).
3. J. M. Meek and J. D. Craggs, eds., *Electrical Breakdown of Gases* (Wiley, New York, 1978).
4. R. J. Nordstrom, "Study of laser-induced plasma emission spectra of N_2, O_2, and ambient air in the region 350 nm to 950 nm," Appl. Spectrosc. **49,** 1490–1499 (1995).
5. J. R. Hollahan and A. T. Bell, eds., *Techniques and Applications of Plasma Chemistry* (Wiley, New York, 1974).
6. L. J. Radziemski and D. A. Cremers, eds., *Laser-Induced Plasmas and Applications* (Marcel Dekker, New York, 1989).
7. A. Borghese, A. D'Alessio, G. Russo, and C. Venitozzi, "Time resolved electrical and spectroscopic study of very short spark discharges," in *Proceedings of the International Symposium on Diagnostics and Modelling of Combustion in Reciprocating Engines* (Japanese Society of Mechanical Engineers, Tokyo, Japan, 1985), pp. 77–83.
8. H. R. Griem, ed., *Plasma Spectroscopy* (McGraw-Hill, 1964).
9. R. H. Huddlestone and S. L. Leonard, eds., *Plasma Diagnostic Techniques* (Academic, New York, 1965).
10. A. Borghese and S. S. Merola, "Time resolved spatial and spectral analysis of a special light source for the broadband extinction spectroscopy technique," in *Proceedings of FRANTIC '97* (Friendly Related Appointments, National and/or Transnational and/or International Congress) (Associazione Sezione Italiana del Combustion Institute, Naples, Italy, 1997), p. IV-3.
11. A. Borghese and S. S. Merola, "Detection of extremely fine carbonaceous particles in the exhausts of diesel and spark-ignited i.c. engines, by means of broadband extinction and scattering spectroscopy in the ultraviolet band 190 nm-400 nm," to be presented at the Twenty-seventh International Symposium on Combustion, Boulder, Colorado, 1998 (Combustion Institute, Pittsburgh, Pa., 1998).
12. S. S. Merola, M. Kurz, A. Borghese, A. D'Anna, and A. D'Alessio, "Ultraviolet broadband light scattering by single metal-containing droplets," Combust. Sci. Technol. (to be published).